THE ASTROPHYSICAL JOURNAL, 280:405–415, 1984 May 1

COMPARATIVE STUDY OF THE LOSS CONE–DRIVEN INSTABILITIES IN THE LOW SOLAR CORONA

R. R. SHARMA AND LOUKAS VLAHOS
Astronomy Program, University of Maryland
Received 1983 March 29; accepted 1983 October 28

ABSTRACT

A comparative study of the loss cone–driven instabilities in the low solar corona is undertaken. The instabilities considered are the electron cyclotron maser, the whistler, and the electrostatic upper hybrid. We show that the first-harmonic extraordinary mode of the electron cyclotron maser instability is the fastest growing mode for strongly magnetized plasma ($\omega_e/\Omega_e < 0.35$, where ω_e is the plasma frequency, and Ω_e is the cyclotron frequency). For $0.35 < \omega_e/\Omega_e < 1.0$, the first-harmonic ordinary mode of the electron cyclotron maser instability dominates the emission. For $\omega_e/\Omega_e > 1.0$, no direct electromagnetic radiation is expected since other instabilities, which do not escape directly, saturate the electron cyclotron maser (the whistler or the electrostatic upper hybrid waves). We also show that the second-harmonic electron cyclotron maser emission never grows to an appreciable level. Thus, we suggest that the electron cyclotron maser instability can be the explanation for intense radio bursts only when the first harmonic escapes from the low corona. We propose a possible explanation for the escape of the first harmonic from a flaring loop.

Subject headings: instabilities — masers — radiation mechanisms — Sun: corona — Sun: flares — Sun: radio radiation

I. INTRODUCTION

Over the past years there has been great interest in solar physics in direct electron cyclotron emission from unstable electron distributions as a possible interpretation of various radio bursts (Twiss and Roberts 1958; Fung and Yip 1966; Ramaty 1969; Mangeney and Veltri 1976; Stepanov 1978). Interest in the direct electron cyclotron maser radiation driven by a loss cone–type distribution formed by the reflected electrons inside a flaring loop was renewed recently (Holman, Eichler, and Kundu 1980; Melrose and Dulk 1982*a*; Sharma, Vlahos, and Papadopoulos 1982, hereafter SVP), motivated by a series of observations with high time and spectral resolution (Slottje 1978, 1980; Zhao and Jin 1982). The importance of the loss cone–driven electron cyclotron maser emission on the overall energetics of the low corona seems to be even more significant than providing energy for the observed radio bursts (Melrose and Dulk 1982*b*). Sprangle and Vlahos (1983) showed that part of the radiation may be reabsorbed by the tail of a thermal distribution outside the magnetic trap and accelerate electrons to high energies.

The electron cyclotron maser instability driven by a loss cone–type velocity distribution was studied extensively several years ago in relation to the terrestrial kilometric radiation (Wu and Lee 1979; Lee and Wu 1980; Lee, Kan, and Wu 1980; Melrose, Rönnmark, and Hewitt 1982) and the decametric radio emission from Jupiter (Hewitt, Melrose, and Rönnmark 1981, 1982). In solar physics, the initial suggestion of Holman, Eichler, and Kundu (1980) that the intense, highly polarized, and "spiky" radio emission observed by Slottje (1978) may be attributed to the electron cyclotron maser instability was followed by several other studies. Melrose and Dulk (1982*a*) claimed that the second-harmonic extraordinary mode (*X*-mode) is the best candidate for the "spiky" radio emission. SVP showed that if the first-harmonic *X*-mode grows and does not escape, the second harmonic will never grow to any appreciable level. That is because the first harmonic will quickly isotropize the velocity distribution before the second harmonic grows above the thermal noise level. The only way that the second-harmonic *X*-mode can grow is when $\omega_e/\Omega_e > 0.4$ and the growth rate of the first-harmonic *X*-mode is comparable to or smaller than the second-harmonic *X*-mode. Melrose and Dulk (1982*a*) reached a similar conclusion. Finally, SVP emphasized the role of thermal damping on the second-harmonic *X*-mode from the emission layer itself. They showed the *second-harmonic X-mode* will not grow if the ambient temperature rises above 5×10^6 K.

Electron cyclotron *absorption* from the ambient plasma plays an important role in the escape of the electromagnetic radiation from the Sun (see Zheleznyakov 1970). Holman, Eichler, and Kundu (1980) claimed that the first-harmonic *X*-mode *can escape* from the Sun through a window at small angles with respect to the magnetic field where the absorption is relatively weak. This point was not pursued further by Holman, Eichler, and Kundu (1980) until today and is worthy of further study. Melrose and Dulk (1982*a*), on the other hand, quoted a formula from Zheleznyakov (1970, p. 454) to support their claim that the second-harmonic *X*-mode will easily escape from the corona. Unfortunately, this formula is valid for quasi-longitudinal propagation only (that is, the wave is propagating nearly along the magnetic field lines). Vlahos, Sharma, and Papadopoulos (1983) repeated the calculation of Zheleznyakov (1970) for arbitrary angle and showed that the thermal absorption drops dramatically at small and large angles of wave propagation with respect to the ambient magnetic field. Finally, SVP pointed out that all the above calculations assumed that the velocity distribution at the resonance layer is Maxwellian. This assumption may not be true inside a flaring loop since a substantial number of nonthermal electrons are present during the impulsive phase of the burst.

The following aspects of the loss cone–driven electron cyclotron maser instability were analyzed in our present study.

1. We study the influence of ω_e/Ω_e and ambient plasma temperature (T_e) in the first- and the second-harmonic X- and O-modes. We vary T_e from 2×10^6 K to 1.0×10^7 K and ω_e/Ω_e from 0.1 to 2.5.

2. We analyze the role that other loss cone–driven instabilities (whistler and electrostatic upper hybrid as well as the slow X-mode electron cyclotron maser) play on the saturation of the electron cyclotron maser emission.

3. We carry out the above analysis with two different velocity distributions in order to examine the role of the velocity distribution on these instabilities.

Our main conclusions from this study are the following:

1. The first-harmonic X-mode from the electron cyclotron maser instability is the fastest growing mode for $\omega_e/\Omega_e < 0.35$ and is not very sensitive to the ambient temperature.

2. For $0.35 < \omega_e/\Omega_e < 1.0$, the first-harmonic O-mode from the electron cyclotron maser emission is the fastest growing mode and is also not very sensitive to T_e.

3. For $\omega_e/\Omega_e > 1.0$, several other instabilities, which cannot escape directly (the whistler instability or the upper hybrid electrostatic instability), are the fastest growing waves and saturate the electron cyclotron maser.

Thus, our main conclusion is that the second-harmonic X- and O-modes never become the fastest growing modes, and *unless the first harmonic escapes from the low corona, the electron cyclotron maser will never become the dominant emission mechanism for any radio burst.* In our previous study (SVP) we did not appreciate the role that the electron cyclotron maser first-harmonic O-mode plays on the saturation of the maser instability, and we reached a different conclusion.

The plan of the paper is as follows: § II treats the electron cyclotron maser instability using two types of distribution functions. The whistler and upper hybrid electrostatic instabilities are discussed in §§ III and IV, respectively. The power and the polarization estimates for typical solar flare parameters are given in § V. Conclusions and discussions are presented in § VI.

II. ELECTRON CYCLOTRON MASER INSTABILITY

We assume that the distribution function of the reflected electrons f_r can be represented by (Dory, Guest, and Harris 1965, hereafter DGH)

$$f_r(v_\parallel, v_\perp) = n_r f_{r\perp}(v_\perp) f_{r\parallel}(v_\parallel) , \tag{1}$$

where

$$f_{r\perp}(v_\perp) = \frac{1}{2\pi} \frac{1.}{\beta_\perp^2 \alpha!} \left(\frac{1}{2}\right)^\alpha \left(\frac{v_\perp}{\beta_\perp}\right)^{2\alpha} \exp\left(\frac{-v_\perp^2}{2\beta_\perp^2}\right) , \tag{2}$$

$$f_{r\parallel}(v_\parallel) = \left(\frac{1}{2\pi}\right)^{1/2} \frac{1}{\beta_\parallel} \exp\left[-\frac{(v_\parallel - v_b)^2}{2\beta_\parallel^2}\right] . \tag{3}$$

Here n_r represents the number of the reflected electrons, and α is the loss cone index which represents the steepness of the distribution function. The quantities $\beta_\perp$ and $\beta_\parallel$ are the thermal velocities in the directions perpendicular and parallel to the static magnetic field, respectively, and are given by $\beta_\perp = (T_\perp/m_e)^{1/2}$, $\beta_\parallel = (T_\parallel/m_e)^{1/2}$; $T_\parallel$ and $T_\perp$ are the electron temperatures parallel and perpendicular to the magnetic field; and v_b is the mean beam velocity in the direction of the magnetic field. The above velocity distribution function has both velocity anisotropy as well as temperature anisotropy. The effective temperature anisotropy ($T_{\rm eff}$) for this distribution is given by

$$T_{\rm eff} = (\alpha + 1) \frac{T_\perp}{T_\parallel} - 1.0 . \tag{4}$$

In order to compute the normalized growth rate, we first define several basic quantities. The streaming energy of the energetic electrons is

$$\epsilon_s = \frac{m_e}{2} v_b^2 ; \tag{5}$$

the parallel energy is given by

$$\epsilon_\parallel = \frac{m_e}{2} \int d^3v (v_\parallel - v_b)^2 f_r = \frac{m_e}{2} \beta_\parallel^2 ; \tag{6}$$

and the perpendicular energy can be defined as

$$\epsilon_\perp = \frac{m_e}{2} \int d^3v v_\perp^2 f_r = m_e \beta_\perp^2 (1 + \alpha) . \tag{7}$$

In the numerical computation which follows, we assume that the streaming energy and the parallel energy are each about 1/10 of the perpendicular energy.

a) *The Plasma Effects*

The importance of the ratio ω_e/Ω_e on the growth rate of the electron cyclotron maser was emphasized in several studies (e.g., Lee and Wu 1980; SVP). In all previous studies, ω_e/Ω_e was varied only between 0.1 and 1, and the emphasis was on the dramatic change of the first-harmonic X-mode growth rate around $\omega_e/\Omega_e = 0.35$. In fact, for $\omega_e/\Omega_e > 0.35$, the second-harmonic X-mode grows faster than the first-harmonic X-mode. In our study here we extend the variation of ω_e/Ω_e from 0.1 to 2.5 since the parameter ω_e/Ω_e is not known in the low corona. Also, ω_e/Ω_e changes with time in the course of a flare inside a flaring loop (because of the heating of the upper chromosphere by precipitating electrons). We define the effective growth rate as

$$\frac{\gamma_{\rm eff}}{\Omega_e} = \frac{\gamma}{\Omega_e} - \frac{\gamma_d}{\Omega_e} , \tag{8}$$

where γ is the growth rate for the electron cyclotron maser instability (given in Appendix A), and γ_d is the thermal damping from the emission layer itself. The effective growth rate is a function of ω_e/Ω_e, the real wave frequency (ω_r), and the angle of propagation of the unstable wave to the ambient magnetic field (ψ). In Figure 1 we plot the maximized effective growth rate ($\gamma_{\rm eff}^{\rm max}/\Omega_e$) as a function of ω_e/Ω_e, which means that we first search for the maximum growth rate in ω_r/Ω_e and ψ space for each ω_e/Ω_e. We use the following numerical parameters: $\epsilon_\perp = 30$ keV, $\epsilon_\parallel = 3$ keV, the loss cone index $\alpha = 1$, $n_r/n_0 = 10^{-2}$, and the ambient thermal temperature = 2.0×10^6 K. It is clear from Figure 1 that for $\omega_e/\Omega_e \lesssim 0.35$, the *first-harmonic X-mode* is the dominant mode. For $0.35 < \omega_e/\Omega_e < 1.0$, the dominant mode is the *first-harmonic O-mode.* The *second-harmonic X-mode* grows faster than the first-harmonic X-mode and the second-harmonic O-mode between 0.35 and 1.0 but *slower than the first-harmonic O-mode by as much as one order of magnitude.* The implications of this will be examined in § IV. For $1.0 < \omega_e/\Omega_e < 1.45$, the *second-harmonic*

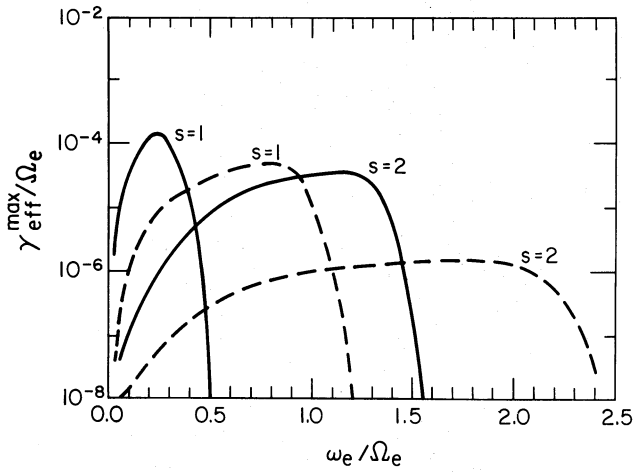

FIG. 1

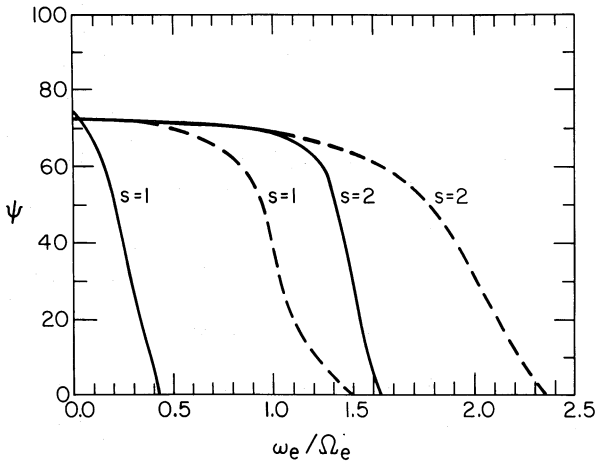

FIG. 2

FIG. 1.—The normalized effective growth rate is plotted as a function of ω_e/Ω_e for the electron cyclotron maser instability. The first and second harmonics for the X-mode (*solid lines*) and O-mode (*dashed lines*) are shown. The following parameters are used in this graph: $\epsilon_\perp = 30$ keV, $\epsilon_s = \epsilon_\parallel = 3$ keV, $\alpha = 1$, $T_e = 2 \times 10^6$ K, $n_r/n_0 = 10^{-2}$.

FIG. 2.—The angle ψ between the direction of the unstable electron cyclotron maser wave and the magnetic field as a function of ω_e/Ω_e is plotted. The first and the second harmonics for the X-mode (*solid lines*) and O-mode (*dashed lines*) are shown. Other parameters are the same as in Fig. 1.

X-mode is the dominant electron cyclotron maser mode. For ω_e/Ω_e ranging from 1.45 to 2.4, the second-harmonic O-mode is the dominant mode.

The variation of ψ at the maximum growth as a function of ω_e/Ω_e is shown in Figure 2. It is also seen that the second harmonic is emitted at considerably larger angles to the magnetic field over a wide range of ω_e/Ω_e as compared to the first harmonic. In the growth rate given in Appendix A, both axial (cyclotron maser instability) and azimuthal bunching (Weibel-like instability) are simultaneously present, and they are the two extremes of the same instability (see Chu and Hirshfield 1978 or Winglee 1983).

b) *The Thermal Damping in the Emission Layer*

In our previous study (SVP) we analyzed the importance of the thermal damping *only for the second-harmonic X-mode*. In our present study we found that the first-harmonic X- and O-modes are not affected by the temperature variations (in the range 2×10^6–1×10^7 K, which is of interest here). Thus we focus our analysis on the second-harmonic X- and O-modes. In Figure 3*a* we plot the effective growth rate for the second-harmonic X-mode as a function of ω_r/Ω_e for different temperatures using $\omega_e/\Omega_e = 1$, and maximized with respect to ψ. Other parameters are the same as in Figure 1. We can see in Figure 3*a* that as the temperature increases, the peak is shifted to larger ω_r/Ω_e. The second-harmonic X-mode is damped for $T_e > 2.0 \times 10^7$ K. This number seems to depend on the details of the velocity distribution (as we will see below) and the ratio n_r/n_0 (here we use $n_r/n_0 = 10^{-2}$). In Figure 3*b* we plot the O-mode second harmonic for the same parameters. We find that the O-mode is also very sensitive to the temperature changes. In Fig. 4 we plot $\gamma_{eff}^{max}/\Omega_e$ as a function of ω_e/Ω_e for

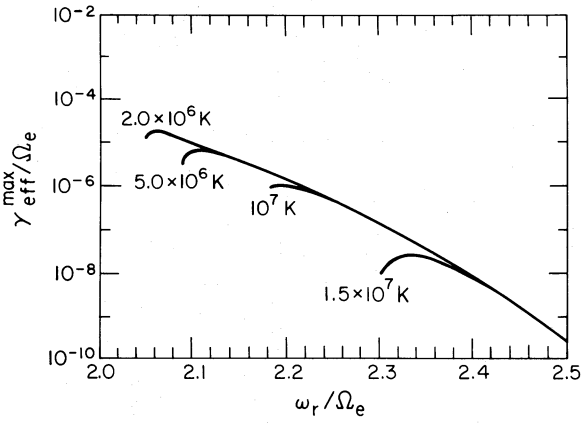

FIG. 3*a*

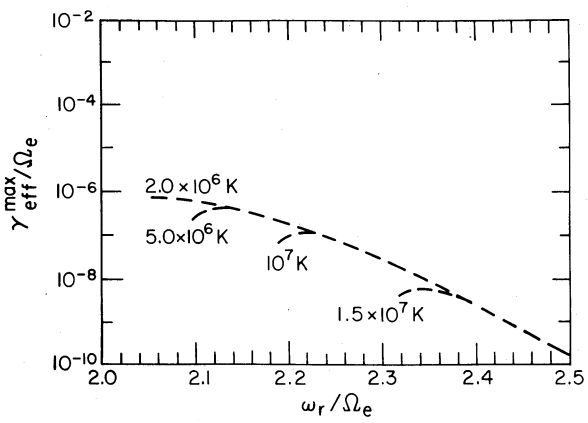

FIG. 3*b*

FIG. 3.—(*a*) The effective growth rate for the X-mode, second-harmonic electron cyclotron maser instability as a function of the real frequency is plotted for different temperatures. The parameters used in this figure are $\epsilon_\perp = 30$ keV, $\epsilon_s = \epsilon_\parallel = 3$ keV, $\alpha = 1$, $n_r/n_0 = 10^{-2}$, and $\omega_e/\Omega_e = 1$. (*b*) As in Fig. 3*a* for the O-mode second harmonic.

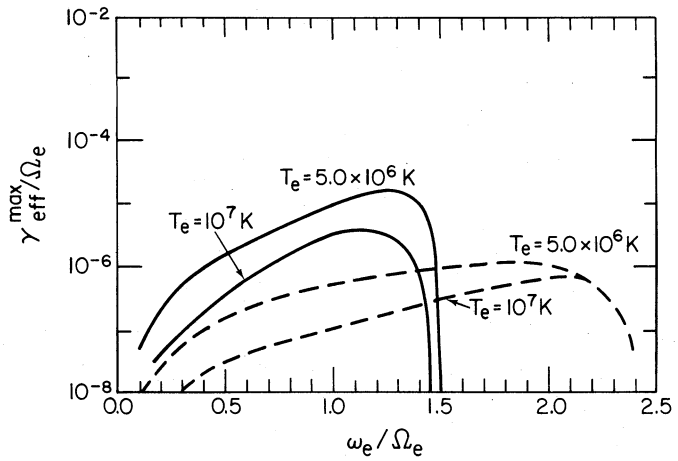

FIG. 4

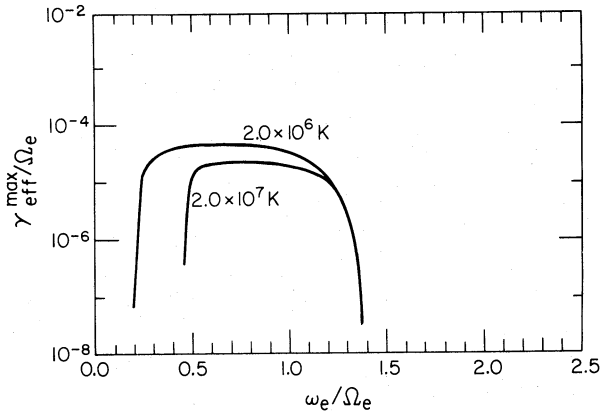

FIG. 5

FIG. 4.—The normalized effective growth rates for the second-harmonic X-mode (*solid lines*) and O-mode (*dashed lines*) of the electron cyclotron maser instability as a function of ω_e/Ω_e for two different temperatures are plotted. The other parameters used in this figure are the same as in Fig. 1.

FIG. 5.—The slow X-mode effective growth rate for the electron cyclotron maser instability as a function of ω_e/Ω_e is plotted. The parameters used are the same as in Fig. 1.

$T_e = 5.0 \times 10^6$ K and 1.0×10^7 K for the second-harmonic X- and O-modes.

c) *The Slow X-Mode*

The slow X-mode (usually called Z-mode) of the electron cyclotron maser instability has been ignored in previous studies since it encounters the stop zone and does not escape directly. Several recent studies have shown that this mode can escape through a direct mode conversion (Jones 1976; Melrose 1980). The slow X-mode is examined here only for the purpose of finding the parameters for which this mode becomes the fastest growing wave and dominates the pitch angle scattering. In Figure 5 we plot the $\gamma^{max}_{eff}/\Omega_e$ for this mode as a function of ω_e/Ω_e for the same parameters as in Fig. 1. This mode grows for ω_e/Ω_e ranging from 0.2 to 1.4. The growth rate is comparable to the first-harmonic O-mode for ω_e/Ω_e ratios lying between 0.4 and 0.6.

d) *Second Loss-Cone Velocity Distribution*

We repeat all the above steps of our analysis with a different velocity distribution given by

$$f_r(v_\parallel, v_\perp) = n_r f_{r\perp}(v_\perp) f_{r\parallel}(v_\parallel) , \tag{9}$$

where

$$f_{e\perp}(v_\perp) = \frac{1}{2\pi} \frac{1}{(\beta^2_{\perp 1} - q\beta^2_{\perp 2})} \left[\exp\left(-\frac{v^2_\perp}{2\beta^2_{\perp 1}} \right) - q \exp\left(\frac{v^2_\perp}{2\beta^2_{\perp 2}} \right) \right] , \tag{10}$$

and $f_{r\parallel}(v_\parallel)$ is given in equation (3). Here, $\beta_{\perp 1}$ and $\beta_{\perp 2}$ are the thermal spreads of the reflected electrons in the perpendicular direction, and q is a free parameter. It is already established (Lee and Wu 1980) that as q decreases from unity, the instability growth decreases as well. It is also known that the reflected electron distribution has maximum positive slope for $q = 1$. Therefore, we let $q = 1.0$ in the numerical computation for the growth rate. The parallel particle energy ($\epsilon_\parallel$), the parallel streaming energy (ϵ_s), and the perpendicular particle energy ($\epsilon_\perp$) are the same as for a DGH type of distribution. Therefore, there is one more parameter T_2/T_1 [where $\beta_{\perp 2} = (T_2/m_e)^{1/2}$, $\beta_{\perp 1} = (T_1/m_e)^{1/2}$] which has to be specified. We took this ratio to be 0.25. Our conclusions for this distribution remain almost the same as for a DGH type of distribution, with the only difference being that the ratio ω_e/Ω_e above which the first- and second-harmonic modes become evanescent is reduced slightly.

III. WHISTLER INSTABILITY

The whistler mode is a right circularly polarized wave which propagates along the direction of the static magnetic field ($\psi = 0$) and has a real frequency range of $\Omega_i < \omega < \Omega_e$ (Ω_i is the ion cyclotron frequency). The growth rate of the whistler wave in the presence of energetic electrons is given in Appendix B. The parameter ω_r/Ω_e ranges from (m_e/m_i) to 0.6 (m_i is the ion mass). The variation of normalized growth rate with respect to the ratio ω_e/Ω_e is shown in Figure 6 for loss cone distributions

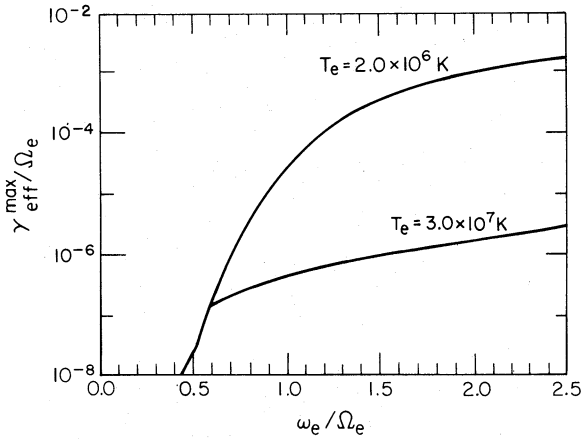

FIG. 6.—The ratio $\gamma^{max}_{eff}/\Omega_e$ as a function of ω_e/Ω_e for the whistler instability is plotted. The parameters used are the same as in Fig. 1.

(DGH) with the following parameters: $\epsilon_\perp = 30$ keV, $\epsilon_\parallel = 3$ keV, $\epsilon_s = 3$ keV, $n_r/n_0 = 10^{-2}$, $\alpha = 1.0$, $T_e = 2.0 \times 10^6$ K. It is clear from Figure 6 that the growth rate for the whistler wave is very small for $\omega_e/\Omega_e \lesssim 0.45$. As the ratio ω_e/Ω_e increases from 0.5 to higher values, the growth rate increases to $10^{-3}\Omega_e$ for $\omega_e/\Omega_e \approx 2.0$. If the temperature of the background plasma becomes 3.0×10^7 K, the effective growth rate for $\omega_e/\Omega_e \approx 2.0$ decreases by three orders of magnitude. Cyclotron damping affects the growth, but the threshold value of ω_e/Ω_e for $\gamma_{\rm eff}^{\rm max} \gtrsim 0$ remains the same. Further increase of temperature decreases the growth rate very much. This mode grows faster than the electron cyclotron maser modes only for $\omega_e/\Omega_e \gtrsim 1.0$ and $T_e = 2.0 \times 10^6$ K. So for $\omega_e/\Omega_e \gtrsim 1.0$, this mode is important for the saturation of the maser instability. The above results remain unchanged if the second distribution function is used. The growth rate for the whistler instability decreases slightly if the full relativistic dispersion relation is used (Gladd 1981).

IV. UPPER HYBRID ELECTROSTATIC INSTABILITY

It is known that upper hybrid electrostatic waves grow faster than all other loss cone–driven electrostatic instabilities (e.g., the electrostatic Bernstein mode; see Zheleznyakov and Zlotnik 1975). We investigate in this section only the upper hybrid electrostatic wave instability. For this mode the wavelength is much larger than the gyroradius of thermal electrons ($\lambda = k^2 v_e^2/\Omega_e^2 \ll 1$). Thus, we employ a cold plasma dispersion relation for the real part of the dielectric function. The growth rate is given by equation (C5) in Appendix C. In the analysis presented here $k_\parallel \gg \omega\beta_\perp/mc^2$, and the relativistic effects do not play a major role in the estimates of the linear growth rate (see Zheleznyakov and Zlotnik 1975). For our numerical calculation of the growth rate we choose the following parameters: $\alpha = 1$, $n_r/n_0 = 10^{-2}$, $\epsilon_\perp = 30$ keV, $\epsilon_\parallel = 3$ keV, $\epsilon_s = 3$ keV, and $T_e = 2.0 \times 10^6$ K. The growth rate (eq. [C5]) does not contain damping and can be self-consistently included by following Goldstein *et al.* (1983) and Vlahos, Sharma, and Papadopoulos (1983). Figure 7 shows the plot of effective normalized growth rate as a function of the ratio ω_e/Ω_e. This mode is damped for $\omega_e/\Omega_e \lesssim 0.25$ but then grows to values as large as (1–5) $\times 10^{-4}\Omega_e$ for $\omega_e/\Omega_e \approx 2.0$. The growth rate for this mode is smaller by at least one order of magnitude as compared to whistler mode growth. Therefore, in the parameter range this mode will never be the fastest growing wave. The loss cone–driven electrostatic upper hybrid instability is important for $\omega_e/\Omega_e > 3.0$, and it can produce strong electromagnetic emission by mode-mode coupling (Stepanov 1974).

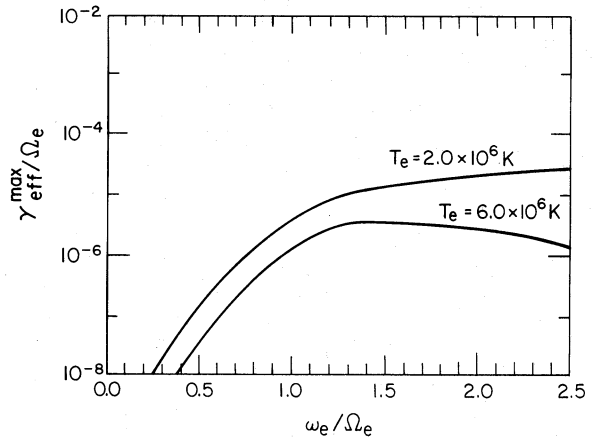

FIG. 7.—The effective growth rate as a function of ω_e/Ω_e for the electrostatic upper hybrid wave is plotted. Other parameters are the same as in Fig. 1.

V. POWER AND POLARIZATION ESTIMATES

In estimating the power received at Earth, from a loss cone velocity distribution formed close to the footpoints of a solar loop in the Sun, the following factors must be taken into account:

1. The first factor is the intensity of the particular mode at the time of the saturation of the loss cone velocity distribution. It was pointed out in SVP that when the electron cyclotron maser instability is the fastest growing wave, the power received at Earth is given by the equation

$$P_j = \frac{W_{sj} V_{{\rm gr}\,j} A_0}{4\pi R_0^2 \Delta f}, \tag{11}$$

where $V_{{\rm gr}\,j}$ is the group velocity of the mode j, A_0 is the surface area of the radiating source, R_0 is the distance of the source from the Earth, Δf is the bandwidth of the radiation, and W_{sj} is the saturation energy density of the growing wave given by (see SVP)

$$W_{sj} = \frac{k_\parallel a}{\Omega_e}\left(\frac{\Omega_e}{\omega_e}\right)^2 \frac{\gamma_j}{\Omega_e} n_0 m_e a^2, \tag{12}$$

where γ_j is the linear growth rate of the particular mode, and a is the average thermal spread. In the case that the fastest growing mode does not escape directly (e.g., slow X-mode or whistler or electrostatic upper hybrid wave), W_{sj} will give us an estimate of the saturation time. We subsequently use this time to estimate the intensity of the wave that escapes directly. In other words, in this case (see SVP)

$$P_j = \frac{I_{sj} V_{{\rm gr}\,j} A_0}{4\pi R_0^2 \Delta f}, \tag{13}$$

where now

$$I_{sj} = I_0 \exp\left(\beta \frac{\gamma_{sj}}{\gamma_2}\right), \tag{14}$$

I_0 is the thermal noise level given by $n_0 T_e (k\lambda_D)^3$, $\lambda_D = v_e/\omega_e$, $\beta = |\ln (W_{sj}/I_0)|$, and γ_2 is the fastest growing mode. If γ_{sj} is the fastest growing wave ($\gamma_{sj} = \gamma_2$), then $I_{sj} = W_{sj}$. We use the analysis presented above and the linear growth rates estimated in the previous sections to plot in Fig. 8 the total power and the polarization using $A_0 = (10^2$ km$)^2$, $\Delta f = 100$ MHz, $k\lambda_D = 10^{-2}$, and $n_r/n_0 \approx 10^{-2}$ (other parameters are the same as in Fig. 1). From this graph we conclude that only the first-harmonic X- and O-modes grow to appreciable level, and the polarization changes sign around $\omega_e/\Omega_e = 0.35$.

The estimates of the power received at Earth change dramatically, from those shown in Figure 8 if we base our analysis only on the electron cyclotron maser instability and ignore all other instabilities. In Figure 9 we plot the power and the polarization for different harmonics using $A_0 = (10^2$ km$)^2$, $\Delta f = 100$ MHz, $n_r/n_0 = 10^{-2}$ (other parameters are the same as in Fig. 1).

2. The next important factor that controls the power that we receive at the Earth from a loss cone–driven instability inside a

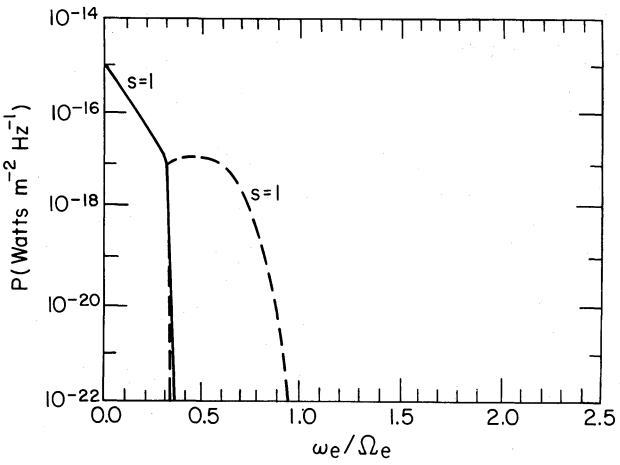

FIG. 8a

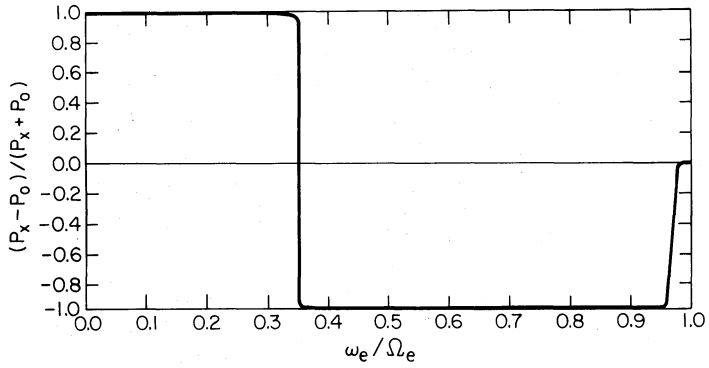

FIG. 8b

FIG. 8.—(*a*) The variation of the power density received at Earth as a function of ω_e/Ω_e. The parameters used are the same as in Fig. 1 except for source area $A_0 = (10^2 \text{ km})^2$, $\Delta f = 10^2$ MHz, $n_0 = 10^{10}$ cm^{-3}, and $k\lambda_D = 10^{-2}$. The solid line is for the *X*-mode, and the dashed line for the *O*-mode. (*b*) The variation of the polarization as a function of ω_e/Ω_e for the same parameters as in Fig. 8*a*.

loop is the absorption or amplification of the radiation by the resonance layers *above the mode under consideration.* It is easy to show that the electron cyclotron maser emission from the first-harmonic *X*- and *O*-modes will be totally absorbed when the resonance layer at frequency $2\Omega_e$ is filled with thermal plasma with temperature 2×10^6 K or higher. One possible way that the first harmonic may escape from the Sun (which was discussed by SVP and Vlahos, Sharma, and Papadopoulos 1983) is when the growth rate at frequency $\omega = 2\Omega_e$ is close to zero or larger [e.g., $\gamma(\omega = 2\Omega_e) \gtrsim 0$] as a result of the presence of nonthermal particles at this level. That is, the second-harmonic layer may emit gyrosynchrotron radiation from an ensemble of trapped nonthermal electrons or may be marginally unstable.

3. Other factors which must be considered in estimating the power received from the loss cone–driven instabilities are the following: (i) The growth length ($L_{\text{gr}\,j} = V_{\text{gr}\,j}/\gamma_j$) for the mode under consideration must be smaller than the size of the volume filled with a loss cone–type velocity distribution. (ii) The power received from the unstable mode must be greater than the gyrosynchrotron emission radiated by the trapped energetic electrons inside the loop. That is, if I_j is smaller than 10^{-20} watts m^{-2} Hz^{-1}, it will be difficult to distinguish the loss cone–driven radiation from the gyrosynchrotron radiation emitted by the trapped energetic electrons.

VI. CONCLUSIONS AND DISCUSSION

Nonthermal electrons accelerated inside the flare volume and streaming toward the low corona will encounter a strong magnetic field and will be reflected (e.g., $v_{\parallel} = 0$). Reflected energetic electrons will form a loss cone–type velocity distribution (since the particles with small pitch angle will have their reflection point inside the dense chromosphere and will lose all their energy by collisions before returning to the corona). The fact that the loss cone distribution is formed close to the transition region has forced us to examine the influence of ω_e/Ω_e and the ambient temperature on the loss cone–driven instabilities. We examined several loss cone–driven instabilities (electron cyclotron maser instability [fast and slow mode], whistler instability, and electrostatic upper hybrid instability) to find out which one is the fastest growing mode for conditions relevant to the low corona (e.g., $0.1 < \omega_e/\Omega_e < 2.5$, 2.0×10^6 K $\leq T_e \lesssim 1.0 \times 10^7$ K). We find that different modes dominate for different values of ω_e/Ω_e. We summarize our results below:

1. Electron cyclotron maser instability dominates the emission for $\omega_e/\Omega_e \lesssim 1$. For $\omega_e/\Omega_e < 0.35$, the first-harmonic *X*-mode is the dominant instability, and for $0.35 < \omega_e/\Omega_e \leq 1.0$, the first-harmonic *O*-mode is the dominant mode. For $\omega_e/\Omega_e > 1.0$, other modes, which do not escape directly, saturate the electron cyclotron maser instability in the second-harmonic *X*- and *O*-modes.

2. The electron cyclotron maser instability will never escape from the low corona if the first harmonic is reabsorbed from the ambient plasma in the second-harmonic resonance level. We suggest that the first-harmonic resonance *can escape* if the second-harmonic level is marginally excited as a result of the presence of a small population of energetic electrons.

3. Finally, we estimated that the thermal damping from the emission layer itself plays an important role only on the growth of the electron cyclotron maser at the second-harmonic *X*-mode, and it effects only slightly the first harmonic (*X*- and *O*-modes). The electron cyclotron maser instability at the second harmonic is very dependent on temperature.

4. The angle ψ for the maximum growth of the electron cyclotron maser emission depends strongly on the parameter ω_e/Ω_e. This dependence is especially strong for the first harmonic (as ω_e/Ω_e increases, ψ decreases to values as small as 5° or smaller).

5. The details of the shape of the velocity distribution have little effect on the conclusions reached above.

The implications of these results for the high time and spectral resolution observations of the low corona are the following:

1. In a flaring loop the ratio ω_e/Ω_e and T_e are time-dependent functions. During the rise part of the burst, they may start with $T_e = 2 \times 10^6$ K and $\omega_e/\Omega_e \lesssim 0.1$ and gradually change to $T_e = 10^7$ K or higher and $\omega_e/\Omega_e > 1$. We expect that the intense "spiky" emission at the first harmonic will be

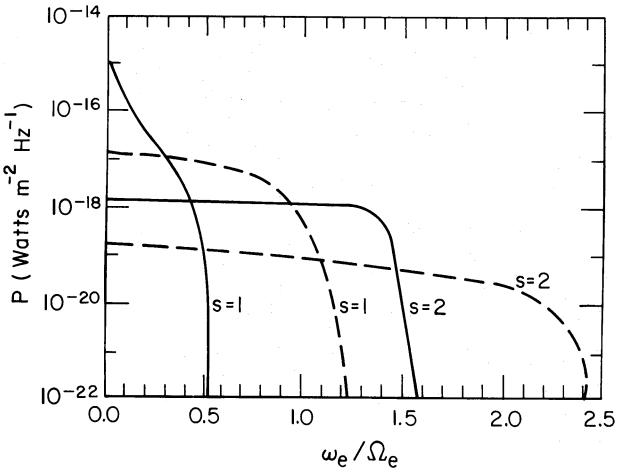

FIG. 9a

FIG. 9.—(*a*) The variation of the power density received at Earth as a function of ω_e/Ω_e (ignoring the saturation by the fastest growing mode). The parameters used are the same as in Fig. 8*a*. The solid lines are for the *X*-mode, and the dashed lines for the *O*-mode. (*b*) The variation of the polarization as a function of ω_e/Ω_e for the parameters of Fig. 8*a*.

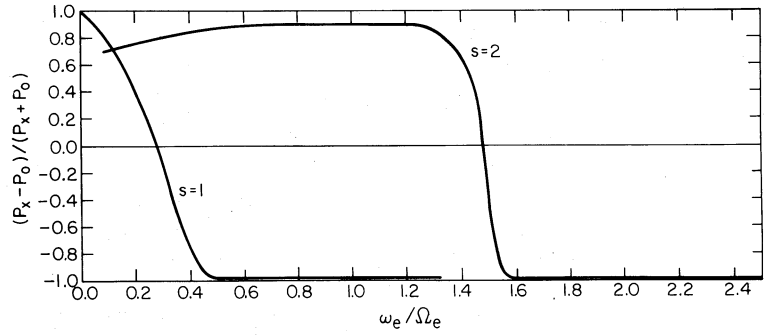

FIG. 9b

observed during the rise of the burst and will disappear when $\omega_e/\Omega_e > 1$ if the electron cyclotron maser emission is the dominant emission mechanism.

2. Depending on the initial value of ω_e/Ω_e, the polarization may change drastically during the event (if ω_e/Ω_e is smaller than 0.35 initially and increases to values larger than 0.35 as the time progresses) or remain unchanged (if $\omega_e/\Omega_e > 0.35$ initially).

We suggest that simultaneous analysis of the high time and spectral resolution data for microwave and dcm radio bursts with EUV and soft X-ray data (which will specify T_e and n_0) may be a useful diagnostic for the presence of loss cone velocity distributions in the low corona.

The authors want to thank Drs. P. Sprangle, M. L. Goldstein, K. Hashimoto, and Professor D. G. Wentzel for stimulating discussions and suggestions. Research was supported by NASA grant NAG W-81. Our numerical computations were partially supported by the Computer Science Center of the University of Maryland.

APPENDIX A

We consider collisionless, uniformly magnetized plasma consisting of a reflected energetic electron component and an ambient background component. The ambient magnetic field is taken along the *z*-direction. We also assume that the density of the reflected electrons is much smaller than the density of the background population. Therefore, the dispersion characteristics are described by the background electrons, and the reflected electrons contribute only to the amplification of the normal modes of the plasma. The amplification is considered within the framework of linearized Vlasov theory. Furthermore, we assume that the frequency is high enough that the ion motion can be neglected. The dispersion equation can be written as the sum of contributions from the background plasma and the reflected electrons as

$$D_r + iD_i = 0 , \tag{A1}$$

where D_r is due to the background population, and D_i is due to the reflected electron population. The thermal effects on the background plasma are ignored if (i) $|\omega - n\Omega_e| \gg k_{\parallel} v_e$ and (ii) $k_{\perp} v_e/\Omega_e \ll 1$ (n is the harmonic number, $k_{\parallel}$ and $k_{\perp}$ are the wave vector components parallel and perpendicular to the static magnetic field B_s, v_e is the thermal velocity of the background electrons,

and $\Omega_e = |e| B_s/m_e c$). The conditions (i) and (ii) are well satisfied for a coronal temperature of 10^8 K and for a wave frequency which is not very close to the gyrofrequency of the electrons. Therefore, for cold plasma, one can write (Akhiezer *et al.* 1967)

$$D_r(\omega, \boldsymbol{k}) = AN^4 - BN^2 + C\,, \tag{A2}$$

where $N = ck/\omega$ is the wave refractive index, and

$$A = K_\perp \sin^2\psi + K_\parallel \cos^2\psi\,, \tag{A3}$$

$$B = K_\parallel K_\perp + AK_\perp - K_H^2 \sin^2\psi\,, \tag{A4}$$

$$C = K_\parallel (K_\perp^2 - K_H^2)\,, \tag{A5}$$

where ψ is the angle between $\boldsymbol{k}$ and the z-axis (the direction of the static magnetic field). The elements of the cold dispersion tensor are given by (ion motion is ignored)

$$K_\perp = 1 - \omega_e^2/(\omega_r^2 - \Omega_e^2)\,, \qquad K_\parallel = 1 - \omega_e^2/\omega_r^2\,, \tag{A6}$$

$$K_H = \omega_e^2 \Omega_e/\omega_r(\omega_r^2 - \Omega_e^2)\,. \tag{A7}$$

Equation (A2) is the well-known dispersion relation for magnetoionic wave modes of a cold plasma in the absence of the reflected electrons. The dispersion relation for the reflected electrons can be written (Harris 1968; Montgomery and Tidman 1964; Cuperman 1981; SVP)

$$D_i = \psi_{xx}\,\mathrm{Im}\,\epsilon^r_{xx} + \psi_{xy}\,\mathrm{Re}\,\epsilon^r_{xy} + \psi_{xz}(\mathrm{Im}\,\epsilon^r_{xz} + \mathrm{Im}\,\epsilon^r_{zx}) + \psi_{yy}\,\mathrm{Im}\,\epsilon^r_{yy} + \psi_{yz}(\mathrm{Re}\,\epsilon^r_{yz} - \mathrm{Re}\,\epsilon^r_{zy}) + \psi_{zz}\,\mathrm{Im}\,\epsilon^r_{zz}\,, \tag{A8}$$

where

$$\begin{aligned}
&\psi_{xx} = N^4 \sin^2\psi - N^2(K_\perp \sin^2\psi + K_\parallel) + K_\parallel K_\perp\,, && \psi_{yy} = -N^2(K_\perp \sin^2\psi + K_\parallel \cos^2\psi) + K_\parallel K_\perp\,,\\
&\psi_{zz} = N^4 \cos^2\psi - N^2 K_\perp(1 + \cos^2\psi) + K_\perp^2 - K_H^2\,, && \psi_{xz} = \psi_{zx} = N^2(N^2 - K_\perp)\sin\psi\cos\psi\,,\\
&\psi_{xy} = 2K_H(K_\parallel - N^2\sin^2\psi)\,, && \psi_{yz} = -\psi_{zy} = N^2 K_H \sin\psi\cos\psi\,,
\end{aligned} \tag{A9}$$

and

$$\boldsymbol{\epsilon}^r(\omega, \boldsymbol{k}) \equiv 2\pi\left(\frac{\omega_e}{\omega_r}\right)^2 \frac{1}{n_0}\int_{-\infty}^{+\infty} dv_\parallel \int_0^\infty \frac{dv_\perp}{\gamma}\,\frac{\mathbf{T}}{[\omega_r - k_\parallel v_\parallel - (n\Omega_e/\gamma)]} \tag{A10}$$

where

$$\mathbf{T} = \begin{bmatrix}
v_\perp^2 U\left[\dfrac{n^2 J_n^2(\lambda)}{\lambda^2}\right] & -iv_\perp^2 U\,\dfrac{n}{\lambda}\,J_n(\lambda)J_n'(\lambda) & v_\perp^2 W\,\dfrac{n}{\lambda}\,J_n^2(\lambda)\\
-iv_\perp^2 U\,\dfrac{n}{\lambda}\,J_n(\lambda)J_n'(\lambda) & v_\perp^2 U J_n^{2\prime}(\lambda) & iv_\perp^2 W J_n(\lambda)J_n'(\lambda)\\
v_\parallel v_\perp U\,\dfrac{n}{\lambda}\,J_n^2(\lambda) & -iv_\parallel v_\perp U J_n(\lambda)J_n'(\lambda) & v_\parallel v_\perp W J_n^2(\lambda)
\end{bmatrix} \tag{A11}$$

$$U = \left[(\omega - k_\parallel v_\parallel)\frac{\partial}{\partial v_\perp} + k_\parallel v_\perp \frac{\partial}{\partial v_\parallel}\right] f_r\,, \tag{A12}$$

$$W = \left[\frac{n\Omega_e}{\gamma}\frac{v_\parallel}{v_\perp}\frac{\partial}{\partial v_\perp} + \left(\omega - \frac{n\Omega_e}{\gamma}\right)\frac{\partial}{\partial v_\parallel}\right] f_r\,, \qquad \lambda = \gamma k_\perp \frac{v_\perp}{\Omega_e}\,, \qquad \gamma = \left(1 - \frac{v^2}{c^2}\right)^{-1/2}\,, \tag{A13}$$

and J_n and J_n' are the Bessel functions of order n and its derivative. The argument of the Bessel function is λ. Equation (A10) is the basic equation which has to be solved for different types of the distribution functions. The growth rate can be obtained from expression

$$\gamma_\pm = -D_i \Big/ \frac{\partial}{\partial\omega_r}[D_r(\omega, \boldsymbol{k})]\Big|_{N^2 = N_\pm^2}\,, \tag{A14}$$

where plus and minus signs correspond to the ordinary and the extraordinary mode.

$$\begin{aligned}
\frac{\partial}{\partial\omega_r} D_r(\omega, k) = \frac{1}{\omega_r}\Bigg\{&2N^4\left[\frac{\omega_e^2\omega_r^2}{(\omega_r^2 - \Omega_e^2)^2}\sin^2\psi + \frac{\omega_e^2}{\omega_r^2}\cos^2\psi\right] + 4N^2\left[\frac{\omega_e^2(\omega_e^2 - \Omega_e^2)}{(\omega_r^2 - \Omega_e^2)^2} - 1 - \frac{\omega_e^2\Omega_e^2\sin^2\psi}{2(\omega_r^2 - \Omega_e^2)^2}\right]\\
&+ 2\left[\left(2 - \frac{\omega_e^2}{\omega_r^2}\right)\left(1 - \frac{\omega_e^2}{\omega_r^2 - \Omega_e^2}\right)^2 - \frac{\omega_e^4\Omega_e^2}{\omega_r^2(\omega_r^2 - \Omega_e^2)^2} + 2\left(1 - \frac{\omega_e^2}{\omega_r^2}\right)^2 \frac{\omega_r^2\omega_e^2}{(\omega_r^2 - \Omega_e^2)^2}\right]\Bigg\}\,.
\end{aligned} \tag{A15}$$

It was shown by SVP that because of the high temperature of the ambient plasma, thermal cyclotron damping, from the emission layer, plays an important role in controlling the frequency range of the emission. The cyclotron damping from the Maxwellian

background can be written as

$$\frac{\gamma_d}{\Omega_e} \approx \left(\frac{\pi}{2}\right)^{1/2}\left(\frac{\omega_e}{\omega_r}\right)^2\left(\frac{\omega_r}{\Omega_e}\right)\sum_n\left(\frac{\omega_r}{k_\parallel v_e}\right) \times \exp\left[-\frac{(\omega_r - n\Omega_e)^2}{2k_\parallel^2 v_e^2}\right][(\psi_{xx}+\psi_{yy}+\psi_{xy})A_{xx}+\psi_{zz}A_{zz}+2\psi_{xz}A_{xz}-2\psi_{yz}A_{xz}]\Big/\left\{\omega_r\frac{\partial}{\partial\omega}[D(\omega,\mathbf{k})]\right\}\Big|_{N^2=N_\pm^2}, \quad \text{(A16)}$$

where

$$A_{xx} \approx \left(\frac{1}{2}\right)^n\left(\frac{k_\perp v_e}{\Omega_e}\right)^{2n-2}\frac{n}{(n-1)!}, \qquad A_{zz} \approx \left(\frac{1}{2}\right)^n\left(\frac{k_\perp v_e}{\Omega_e}\right)^{2n}\left(\frac{\omega_r - n\Omega_e}{k_\parallel v_e}\right)^2\frac{1}{n!},$$
$$A_{xz} \approx \left(\frac{1}{2}\right)^n\left(\frac{k_\perp v_e}{\Omega_e}\right)^{2n-1}\left(\frac{\omega_r - n\Omega_e}{k_\parallel v_e}\right)\frac{n}{n!}. \quad \text{(A17)}$$

APPENDIX B

For a wave propagating along the direction of the static magnetic field, the wave equation for transverse components of the electric field can be written as

$$(\epsilon_{xx} - N^2)E_x + \epsilon_{xy}E_y = 0, \quad \text{(B1)}$$
$$-\epsilon_{xy}E_x + (\epsilon_{xx} - N^2)E_y = 0. \quad \text{(B2)}$$

The above equation could be written in the form

$$(\epsilon_{xx} - N^2 - i\epsilon_{xy})(E_x + iE_y) = 0, \quad \text{(B3)}$$
$$(\epsilon_{xx} - N^2 + i\epsilon_{xy})(E_x - iE_y) = 0. \quad \text{(B4)}$$

For right circularly polarized waves, $E_x + iE_y = 0$; therefore, the dispersion relation for these waves becomes

$$\epsilon_{xx} - N^2 + i\epsilon_{xy} = 0. \quad \text{(B5)}$$

This equation can be written for real and imaginary parts as

$$D_r + iD_i = 0, \quad \text{(B6)}$$

where

$$D_r = K_\perp - N^2 - K_H, \quad \text{(B7)}$$
$$D_i = \text{Im}\,\epsilon^r_{xx} + \text{Re}\,\epsilon^r_{xy}, \quad \text{(B8)}$$
$$\text{Im}\,\epsilon^r_{xx} = \text{Re}\,\epsilon^r_{xy}, \quad \text{(B9)}$$
$$\text{Im}\,\epsilon^r_{xx} = -\frac{4\pi e^2}{m_e}\frac{\pi}{\omega_r^2}\left(\frac{1}{2}\right)\iiint\left[(\omega_r - kv_\parallel)\frac{\partial f_0}{\partial v_\perp} + kv_\perp\frac{\partial f_0}{\partial v_\parallel}\right]v_\perp d^3\mathbf{v}\,\delta(\omega_r - kv_\parallel - \Omega_e). \quad \text{(B10)}$$

The growth rate for the whistler wave can be obtained from equation (B6) as

$$\gamma = -D_i\Big/\frac{\partial D_r}{\partial\omega_r}\Big|_{N=N_R} \quad \text{(B11)}$$

Using equations (B7)–(B10), equation (B11) becomes

$$\gamma = \frac{\omega_e^2}{\omega_r}\frac{1}{n_0}\frac{2\pi^2}{G}\iiint\left[(\omega_r - kv_\parallel)\frac{\partial f_r}{\partial v_\perp} + kv_\perp\frac{\partial f_r}{\partial v_\parallel}\right]v_\perp^2\,dv_\perp\,dv_\parallel\,\delta(\omega_r - kv_\parallel - \Omega_e), \quad \text{(B12)}$$

where

$$G = \frac{\omega_e^2(2\omega_r - \Omega_e)}{\omega_r(\omega_r - \Omega_e)^2} + 2N_R^2, \qquad N_R = \left\{1 + \frac{\omega_e^2}{\Omega_e\omega_r[1 - (\omega_r/\Omega_e)]}\right\}^{1/2}.$$

Equation (B12) for the DGH type of distribution becomes

$$\frac{\gamma}{\Omega_e} = \left(\frac{\pi}{2}\right)^{1/2}\frac{\omega_e^2}{\omega_r\Omega_e}\frac{n_r}{n_0}\frac{2}{\alpha!}\frac{1}{G}\exp\left[-\frac{(\omega - \Omega_e - kv_b)^2}{2k^2\beta_\parallel^2}\right]\left\{\alpha\frac{\Omega_e}{k\beta_\parallel}\alpha! - \left[\frac{\Omega_e}{k\beta_\parallel} + \frac{\beta_\perp^2}{\beta_\parallel^2}\frac{(\omega_r - kv_b - \Omega_e)}{k\beta_\parallel}\right](\alpha+1)!\right\}. \quad \text{(B13)}$$

Similarly one can calculate the cyclotron damping from thermal background as

$$\frac{\gamma_d}{\Omega_e} = \left(\frac{\pi}{2}\right)^{1/2}\frac{\omega_e^2}{\omega_r\Omega_e}\frac{\omega_r}{kv_e}\exp\left[-\frac{(\omega_r - \Omega_e)^2}{2k^2v_e^2}\right]. \quad \text{(B14)}$$

APPENDIX C

The dispersion relation for electrostatic upper hybrid waves in the presence of energetic electrons with a nonequilibrium velocity distribution takes the form

$$\epsilon_{\parallel} = \epsilon_{\parallel}^{(0)} + \epsilon_{\parallel}^{(1)} , \tag{C1}$$

where $\epsilon_{\parallel}^{(1)}$ is the contribution of the nonequilibrium component to the longitudinal dielectric permittivity, and $\epsilon_{\parallel}^{(0)}$ is the contribution of the equilibrium component to the longitudinal dielectric permittivity. The growth rate for this instability is given by

$$\gamma = - \frac{\text{Im } \epsilon_{\parallel}^{(1)}}{(\partial/\partial\omega)(\epsilon_{\parallel}^{0})|_{\epsilon_{\parallel}^{(0)}=0}} , \tag{C2}$$

where

$$\text{Im } \epsilon_{\parallel}^{(1)} = - \frac{\omega_e^2}{k^2} \frac{2\pi^2}{n_0} \frac{n_r}{} \sum_n \int_0^{\infty} v_{\perp} J_n^2 \left(- \frac{k_{\perp} v_{\perp}}{\Omega_e} \right) \left(\frac{\partial}{\partial v_{\parallel}} - \frac{n\Omega_e}{k_{\parallel} v_{\perp}} \frac{\partial}{\partial v_{\perp}} \right) f_r \Big|_{v_{\parallel} = (\omega_r + n\Omega_e)/k_{\parallel}} . \tag{C3}$$

Here, $\epsilon_{\parallel}^{(0)}$ for cold background plasma could be written as

$$\epsilon_{\parallel}^{(0)} = 1 - \frac{\omega_e^2}{\omega_r^2 - \Omega_e^2} \sin^2 \psi - \frac{\omega_e^2}{\omega_r^2} \cos^2 \psi . \tag{C4}$$

Using equations (C3) and (C4) in equation (C2), the growth rate for the DGH type of distribution can be written as

$$\frac{\gamma}{\Omega_e} = \frac{(\pi/2)^{1/2}}{S_1} \frac{\omega_e^2}{k^2 \beta_{\perp}^2} \frac{n_r}{n_0} \frac{1}{\alpha!} \sum_n \frac{n\Omega_e}{k_{\parallel} \beta_{\parallel}} \exp \left[- \frac{(\omega_r + n\Omega_e - k_{\parallel} v_b)^2}{2k_{\parallel}^2 \beta_{\parallel}^2} \right] (I_1 - I_2) , \tag{C5}$$

where

$$I_1 = \left[1 - \frac{\beta_{\perp}^2}{\beta_{\parallel}^2} \frac{(\omega_r + n\Omega_e - k_{\parallel} v_b)}{n\Omega_e} \right] \int_0^{\infty} x^{\alpha} e^{-x} J_n^2 \left(2^{1/2} \frac{k_{\perp} \beta_{\perp}}{\Omega_e} x^{1/2} \right) dx ,$$

$$I_2 = \alpha \int_0^{\infty} x^{\alpha - 1} e^{-x} J_n^2 \left(2^{1/2} \frac{k_{\perp} \beta_{\perp}}{\Omega_e} x^{1/2} \right) dx ,$$

and

$$S_1 = \frac{2(\omega_e^2/\Omega_e^2)}{(\omega_r/\Omega_e)^3 [(\omega_r/\Omega_e)^2 - 1]^2} \left[\left(\frac{\omega_r}{\Omega_e} \right)^4 + \cos^2 \psi - 2 \left(\frac{\omega_r}{\Omega_e} \right)^2 \cos^2 \psi \right] ,$$

$$\left(\frac{\omega_r}{\Omega_e} \right)^2 = \frac{1}{2} \left\{ \left(\frac{\omega_e^2}{\Omega_e^2} + 1 \right) + \left[\left(1 + \frac{\omega_e^2}{\Omega_e^2} \right)^2 - 4 \left(\frac{\omega_e}{\Omega_e} \right)^2 \cos^2 \psi \right]^{1/2} \right\} . \tag{C6}$$

For the difference of two Maxwellian distributions (DTM), equation (C2) becomes

$$\frac{\gamma}{\Omega_e} = \frac{(\pi/2)^{1/2}}{S_1} \frac{\omega_e^2}{k^2 \beta_{\perp 1}^2} \frac{n_r}{n_0} \frac{1}{[1 - q(\beta_{\perp 2}/\beta_{\perp 1})^2]} \left(\frac{c}{\beta_{\perp 1}} \right)^2 \sum \frac{n\Omega_e}{k_{\parallel} \beta_{\parallel}} \exp \left[- \frac{(\omega_r + n\Omega_e - k_{\parallel} v_b)^2}{2k_{\parallel}^2 \beta_{\parallel}^2} \right] (I_3 - I_4) , \tag{C7}$$

where

$$I_3 = \left[1 - \left(\frac{\beta_{\perp 1}}{\beta_{\parallel}} \right)^2 \frac{(\omega_r + n\Omega_e - k_{\parallel} v_b)}{n\Omega_e} \right] \int_0^{\infty} e^{-x} J_n^2 \left(2^{1/2} \frac{k_{\perp} \beta_{\perp 1}}{\Omega_e} x^{1/2} \right) dx ,$$

$$I_4 = q \left[1 - \left(\frac{\beta_{\perp 2}}{\beta_{\perp 1}} \right)^2 \frac{(\omega_r + n\Omega_e - k_{\parallel} v_b)}{n\Omega_e} \right] \int_0^{\infty} e^{-x} J_n^2 \left(2^{1/2} \frac{k_{\perp} \beta_{\perp 2}}{\Omega_e} x^{1/2} \right) dx .$$

REFERENCES

Akhiezer, A. I., Akhiezar, I. A., Polovin, R. V., Sitenko, A. G., and Stepanov, K. N. 1967, *Collective Oscillations in a Plasma* (Oxford: Pergamon Press), Chap. 2.

Chu, K. R., and Hirshfield, J. L. 1978, *Phys. Fluids*, **21**, 461.

Cuperman, S. 1981, *Rev. Geophys. Space Phys.*, **19**, 37.

Dory, R. A., Guest, G. E., and Harris, E. G. 1965, *Phys. Rev. Letters*, **14**, 131 (DGH).

Fung, P. C. W., and Yip, W. K. 1966, *Australian J. Phys.*, **19**, 759.

Gladd, N. T. 1981, paper presented at Second ETB Ring Physics Workshop, San Diego, California, Dec. 1–3.

Goldstein, M., Sharma, R. R., Ben-Ari, M., Eviatar, E., and Papadopoulos, K. 1983, *J. Geophys. Res.*, **88**, 792.

Harris, E. G. 1968, in *Physics of Hot Plasmas*, ed. B. J. Rye and J. C. Taylor (New York: Plenum Press).

Hewitt, R.G., Melrose, D. B., and Rönnmark, K. G. 1981, *Proc. Astr. Soc. Australia*, **1**, 221.

Hewitt, R. G., Melrose, D. B., and Rönnmark, K. G. 1982, *Australian J. Phys.*, **35**, 447.

Holman, G. D., Eichler, D., and Kundu, M. R. 1980, in *IAU Symposium 86, Radio Physics of the Sun*, ed. M. Kundu and T. Gergely (Dordrecht: Reidel), p. 465.

Jones, D. 1976, *Nature*, **260**, 686.

Lee, L. C., Kan, J. R., and Wu, C. S. 1980, *Planet. Space Sci.*, **28**, 703.

Lee, L. C., and Wu, C. S. 1980, *Phys. Fluids*, **23**, 1348.

Mangeney, A., and Veltri, P. 1976, *Astr. Ap.*, **47**, 165.

Melrose, D. B. 1980, *Australian J. Phys.*, **33**, 121.

Melrose, D. B., and Dulk, G. A. 1982*a*, *Ap. J.*, **259**, 844.

———. 1982*b*, *Ap. J. (Letters)*, **259**, L41.

Melrose, D. B., Rönnmark, K. G., and Hewitt, R. G. 1982, *J. Geophys. Res.*, **87**, 5140.

Montgomery, D. C., and Tidman, D. A. 1964, *Plasma Kinetic Theory* (New York: McGraw-Hill).

Ramaty, R. 1969, *Ap. J.*, **178**, 241.
Sharma, R. R., Vlahos, L., and Papadopoulos, K. 1982, *Astr. Ap.*, **112**, 377 (SVP).
Slottje, C. 1978, *Nature*, **275**, 520.
———. 1980, in *IAU Symposium 86, Radio Physics of the Sun*, ed. M. Kundu and T. Gergely (Dordrecht: Reidel), p. 195.
Sprangle, P., and Vlahos, L. 1983, *Ap. J. (Letters)*, **273**, L95.
Stepanov, A. V. 1974, *Soviet Astr.*, **17**, 781.
———. 1978, *Soviet Astr. Letters*, **4**, 103.
Twiss, R. Q., and Roberts, J. A. 1958, *Australian J. Phys.*, **11**, 424.
Vlahos, L., Sharma, R. R., and Papadopoulos, K. 1983, *Ap. J.*, **275**, 374.
Winglee, R. M. 1983, *Plasma Phys.*, **25**, 217.
Wu, C. S., and Lee, L. C. 1979, *Ap. J.*, **230**, 621.
Zhao, R., and Jin, S. 1982, *Sci. Sinica, Ser. A*, **25**, 422.
Zheleznyakov, V. V. 1970, *Radio Emission of the Sun and Planets* (Oxford: Pergamon Press).
Zheleznyakov, V. V., and Zlotnik, E. Y. A. 1975, *Solar Phys.*, **43**, 431.

R. R. SHARMA and L. VLAHOS: Astronomy Program, University of Maryland, College Park, MD 20742